

# Lagrangian transport through an ocean front in the North-Western Mediterranean Sea

Ana M. Mancho

Instituto de Matemáticas y Física Fundamental,  
Consejo Superior de Investigaciones Científicas (CSIC),  
Serrano 121, 28006 Madrid, Spain

Emilio Hernández-García

Instituto Mediterráneo de Estudios Avanzados,  
IMEDEA (CSIC - Universitat de les Illes Balears)  
E-07122 Palma de Mallorca, Spain

Des Small and Stephen Wiggins

School of Mathematics, University of Bristol,  
Bristol BS8 1TW, United Kingdom

Vicente Fernández

Istituto Nazionale di Geofisica e Vulcanologia INGV,  
Via Donato Creti 12, 40128 Bologna, Italy

June 29, 2006

## Abstract

We analyze with the tools of lobe dynamics the velocity field from a numerical simulation of the surface circulation in the Northwestern Mediterranean Sea. We identify relevant hyperbolic trajectories and their manifolds, and show that the transport mechanism known as the ‘turnstile’, previously identified in abstract dynamical systems and simplified model flows, is also at work in this complex and rather realistic ocean flow. In addition nonlinear dynamics techniques are shown to be powerful enough to identify the key geometric structures in this part of the Mediterranean. In particular the North Balearic Front, the westernmost part of the transition zone between saltier and fresher waters in the Western Mediterranean is interpreted in terms of the presence of a semipermanent “Lagrangian barrier” across which little transport occurs. Our construction also reveals the routes along which this transport happens. Topological changes in that picture, associated with the crossing by eddies and that may be interpreted as the breakdown of the front, are also observed during the simulation.

# 1 Introduction

Ocean water masses of different origins have distinct contents of salt, heat, nutrients and chemicals. Currents transport them, and energetic mesoscale features are responsible for most of their mixing with surrounding waters.

Vortices are the most well studied of such structures. Frequently they are long lived, and their cores remain relatively protected from the neighboring areas, so that water trapped inside could maintain its biogeochemical properties for long time, being transported with the vortex. In steady horizontal velocity fields, the centers of vortices are readily identified as elliptic points in the streamfunction level sets. The presence of closed streamlines around them is the mathematical reason for the isolation of the vortex core from the exterior fluid.

When the velocity field changes in time, closed streamlines are replaced by more complex structures, some of which can be related in idealized cases to the Kolmogorov-Arnold-Moser tori of dynamical systems theory. For slowly varying velocity fields vortex cores remain coherent during some time, but there is vigorous stirring of the surrounding fluid that finally leads to water mixing. In order to understand this mixing process, one should focus on features of the velocity field different from the elliptic points characterizing the vortex cores. Since some time ago (Ju et al. 2003; Ide et al. 2002; Mancho et al. 2004) hyperbolic trajectories (trajectories with saddle-like stability properties which are solutions to a dynamical system) have been recognized as the structures responsible for most of the stretching and generation of intertwined small scales that finally leads to mixing. In particular there are *Distinguished Hyperbolic Trajectories* (DHTs), characterized by its special persistence as compared with the other hyperbolic structures, that act as the organizing centers of the fluid stirring processes.

Despite the great amount of attention devoted to the identification and characterization of vortices and their dynamics in oceanographic contexts (Olson 1991; Puillat et al. 2002; Ruiz et al. 2002; Isern-Fontanet et al. 2006), there are few studies focussed on hyperbolic objects, and most of them in idealized settings. A possible reason for this may be

that the intrinsic instability of trajectories close to hyperbolic points makes more difficult their identification, in contrast with the recurrent character of trajectories in vortices that allow their tracking for long times from in situ and satellite measurements. In addition, whereas many aspects of vortex dynamics can be analyzed in a Eulerian framework, hyperbolic trajectories are defined by their Lagrangian characteristics and only in this frame can they be fully characterized (Ide et al. 2002; Mancho et al. 2004).

In this Paper we identify relevant hyperbolic trajectories from the surface velocity field of the Western Mediterranean Sea, obtained from a three dimensional model simulation under climatological atmospheric forcing. Our aim is to show that transport mechanisms, in particular the so called 'turnstile' mechanism, previously identified in abstract dynamical systems (Channon and Lebowitz 1980; Bartlett 1982; MacKay et al. 1984; Wiggins 1992), and discussed in the context of rather simple model flows (Rom-Kedar et al. 1990; Beigie et al. 1994; Samelson 1992; Duan and Wiggins 1996), are also at work in this complex and rather realistic ocean flow. More broadly, nonlinear dynamics techniques are shown to be powerful enough to identify the key geometric structures in this part of the Mediterranean.

Western Mediterranean surface layers (up to a depth of about 150 m) contain Modified Atlantic Waters of rather different characteristics (Millot 1999). Fresher waters (salinity about 36.5 psu) recently entered from the Atlantic occupy the Algerian Basin at the South and older and saltier waters (salinity above 38 psu) occupy the Northern part of the area. The dynamics of the contact zone between these two surface water masses, and eventually their mixing, is important to understand the physical and biogeochemical properties of the Western Mediterranean. We focus on one of the oceanographic structures known to be of importance in these processes, the so-called North Balearic Front (López-García et al. 1994; Pinot et al. 1995; Millot 1999). It extends roughly along the Southwest-Northeast direction at the North of the Balearic Islands, with significant displacements and deformations. It is characterized by a strong salinity jump of about 0.6 psu (37.4 psu to the South and 38.0 to the North) down to 150 m depth. This identifies the front as the main transition zone between the two water masses. In Winter a weak but

detectable temperature gradient of 0.5-1 K/5 km can be observed in satellite images.

After selecting an interval of time in our simulation during which the front is well formed, we explore the transport properties of the surface velocity field in the region, and find the relevant Lagrangian structures, hyperbolic points and their manifolds, responsible for the establishment and permanence of the front. The location of the front is identified as a “Lagrangian barrier” across which transport is small (as quantified with the tools of lobe dynamics), and occurs via filaments that entrain water along transport routes that we identify. The presence of eddies strongly affect the Lagrangian structures in a process that can be interpreted as the break-down of the front.

The Paper is organized as follows: In Section 2 we introduce some of the dynamical systems concepts that will be used in the following. Section 3 describes our numerical ocean model and Section 4 addresses the adaptation of the standard algorithms to the kind of oceanographic data provided by the model. Section 5 contain our main results and the conclusions are summarized in Section 6.

## **2 Distinguished Hyperbolic Trajectories and their Manifolds**

In recent years there have been many applications of the dynamical systems approach to transport in oceanographic flows. Recent reviews are Jones and Winkler (2002); Wiggins (2005); Samelson and Wiggins (2006). In this section we describe the basic ideas that we will use in our analysis. Although the same concepts are of use in three dimensional flows, we describe here just the two dimensional situation, since as discussed below the structures we identify can be considered two dimensional to a good approximation during the time scales relevant here.

Stagnation points are well known features of steady flows that generally play an important role in “organizing” the qualitatively distinct streamlines in the flow. For example, saddle-type stagnation points can occur on boundaries where streams of flow tan-

gential to the boundary coming from opposite directions meet and then separate from that boundary. Saddle-type stagnation points can occur in the interior of a flow at a point where fluid seems to both converge to the point along two opposite directions and diverge from it along two different directions. In steady flows the stagnation point is a trivial example of a fluid particle trajectory (i.e., it is a “solution,” in this case a fixed point solution, of the equations for fluid particle motions defined by the velocity field) and the saddle point nature is manifested by the fact that there are directions for which nearby trajectories approach the stagnation point at an exponential rate and move away from the stagnation point at an exponential rate. These directions are sometimes referred to as “stagnation streamlines”. They define material curves that “cross” at the stagnation point and typically form the boundaries between qualitatively distinct regions of flow.

A related “time-dependent” picture as that described above exists for unsteady flows, with both similar, as well as much more complex, implications for transport. In unsteady flows a stagnation point *at a given time* –or rather, an *Instantaneous Stagnation Point* (ISP)– is a location at which velocity vanishes *at that time*. The sequence of locations is generally *not* a fluid particle trajectory (Ide et al. 2002). The true analog of the saddle-type stagnation point of steady flows is a *Distinguished Hyperbolic Trajectory* (DHT) (Ide et al. 2002). “Hyperbolic” is the dynamical systems terminology for “saddle-type”. These are fluid particle trajectories that have (time-dependent) directions for which nearby trajectories approach and move away from the DHT at exponential rates. “Distinguished” is a notion that is discussed in detail in Ide et al. (2002), but the idea is that these are the key, *isolated* hyperbolic trajectories that serve to organize the transport behavior in a flow because they remain substantially more localized (in a well defined sense, see Ide et al. (2002)) than neighboring hyperbolic trajectories. Ide et al. (2002), Ju et al. (2003), and Mancho et al. (2004) develop the algorithms that allow us to compute DHTs in a given flow. They are iterative methods that start with a first guess for the DHT positions in an interval of time (i.e. an initial curve in space and time) and then refine the space-time curve by imposing the criteria of hyperbolicity and localization. In the flows considered here, a good first guess is the location of ISPs, since it turns out that a DHT is often found

in the neighborhood of an Eulerian ISP.

Just as in the steady case, there are analogs to the stagnation streamlines: in the dynamical systems terminology these are referred to as the *stable and unstable manifolds of the DHT*, and they are time-dependent material curves. In dynamical systems terminology the fact that they are material curves means that they are *invariant*, i.e. a fluid particle trajectory starting on one of these curves must remain on that material curve during the course of its time evolution. “Stable manifold” means that trajectories starting on this material curve approach the DHT at an exponential rate as time goes to infinity, and “unstable manifold” means that trajectories starting on this material curve approach the DHT at an exponential rate as time goes to minus infinity. Mancho et al. (2003, 2004) develop the algorithms that enable us to compute the stable and unstable manifolds of hyperbolic trajectories.

In unsteady flows stable and unstable manifolds of DHTs can intersect in isolated points different from the DHTs. This is a fundamental difference with respect to steady flows, and give rise to moving regions of fluid bounded by pieces of stable and unstable manifolds, the so called “lobes”. Since the manifolds are material lines, fluid can not cross them by purely advective processes and thus they are perfect Lagrangian barriers (diffusion, or motion along the third dimension can however induce cross-manifold transport). Motion of the “lobes” is thus the mechanism responsible for mediating Lagrangian transport between different regions. References describing “lobe dynamics” in general are Rom-Kedar and Wiggins (1990); Beigie et al. (1994); Wiggins (1992); Malhotra and Wiggins (1998); Samelson and Wiggins (2006). Examples of applications of lobe dynamics to oceanographic flows are Ngan and Shepherd (1997); Rogerson et al. (1999); Yuan et al. (2001, 2004); Miller et al. (2002); Deese et al. (2002). We will describe these ideas more fully in the context of transport associated with the Balearic front in the Mediterranean.

### 3 The Ocean Circulation Model

In this work we analyze velocity fields which are obtained from an ocean model, DieCAST (Dietrich 1997), adapted to the Mediterranean Sea (Dietrich et al. 2004; Fernández et al. 2005). The 3D primitive equations are discretized with a fourth-order collocated control volume method. In zones adjacent to boundaries a conventional second order method is used. A fundamental feature of control volume based models is that the predicted quantities are control volume averages, while face-averaged quantities are used to evaluate fluxes across control volume faces (Sanderson and Brassington 1998). These quantities are computed using fourth-order approximations and numerical dispersion errors are further reduced in the modified incompressibility algorithm by Dietrich (1997).

Horizontal resolution is the same in both the longitudinal ( $\phi$ ) and latitudinal ( $\lambda$ ) directions, with  $\Delta\phi = (1/8)$  of degree and  $\Delta\lambda = \cos\lambda\Delta\phi$  thus making square horizontal control volume boundaries. Vertical resolution is variable, with 30 control volume layers. The thickness of control volumes in the top layer is 10.3 m and they are smoothly increased up to the deepest bottom control volume face at 2750 m. Thus ETOP05 bathymetry is truncated at 2750 m depth and it is not filtered or smoothed.

Horizontal viscosity and diffusivity values are constant and equal to  $10 \text{ m}^2 \text{ s}^{-1}$ . For the vertical viscosity and diffusivity, a formulation based on the Richardson number developed in Pacanowski and Philander (1981) is used, with background values set at near-molecular values ( $10^{-6}$  and  $2 \times 10^{-7} \text{ m}^2\text{s}^{-1}$  respectively). We use monthly mean wind stress reanalyzed from 10 m wind output from ECMWF, as chosen for the Mediterranean Sea Models Evaluation Experiment (Beckers et al. 2002). The heat and the freshwater fluxes used to force the model are model-determined from monthly climatological SST and SSS as described in Dietrich et al. (2004). The only open boundary is the Strait of Gibraltar, where inflow conditions are set similar to observations and outflow is model-determined by upwind. Everywhere else, free-slip lateral boundary conditions are used. All bottom dissipation is represented by a conventional nonlinear bottom drag with a coefficient of 0.002. Lateral and bottom boundaries are thermally insulating. The model is



initialized at a state of rest with the annual mean temperature and salinity fields taken from the climatological data. The spin-up phase of integration is carried out for 16 years. Each year is considered to have 12 months 30 days length each (i.e. 360 days). The climatological forcings we use are adequate to identify the mechanisms and processes occurring under typical or average circumstances. Under this approach, high frequency motions are weak in our model and a daily sampling is adequate. The impact on transport of disturbances containing high frequencies, such as storms or wind bursts, is not the focus of the present Paper and would need specific modelling beyond climatological forcing.

We focus on velocity fields obtained at the second layer which has its center at a depth of 15.93 m. This is representative of the surface circulation and is not as directly driven by wind as the top layer. We have recorded velocities, temperatures and salinities in this model layer for five years. Dynamical systems approaches have already been applied to this data set, in particular Lyapunov techniques to quantify mixing strength (d'Ovidio et al. 2004), and the "leaking" approach (Schneider et al. 2005) to quantify escape and residence times in several areas. Here we concentrate in the Northwestern region and apply the methods of lobe dynamics to characterize transport processes in the North Balearic Front area.

Figure 1 shows an example of the output of the model for the velocity field in the selected layer of the Western Mediterranean Sea at day 649 (the 19th day of the tenth month –October– of the second year). Two well known currents, the Northern Current flowing southwards close to the Spanish coast and the Balearic Current associated with the North Balearic Front and flowing northeastwards North of the Balearics, are observed although significantly deformed by the presence of eddies. The Figure shows also the ISPs of the velocity field: circles for the elliptic and crosses for the saddle-type ones.

The velocity field has small vertical components, so that this is not strictly a two dimensional flow. With vertical velocities of the order of  $10^{-5}$  m/s, particles in the second model layer require about 13 days to traverse the layer. But during that time this vertical velocity is not constant. Averaging over the relevant time scales we find effec-

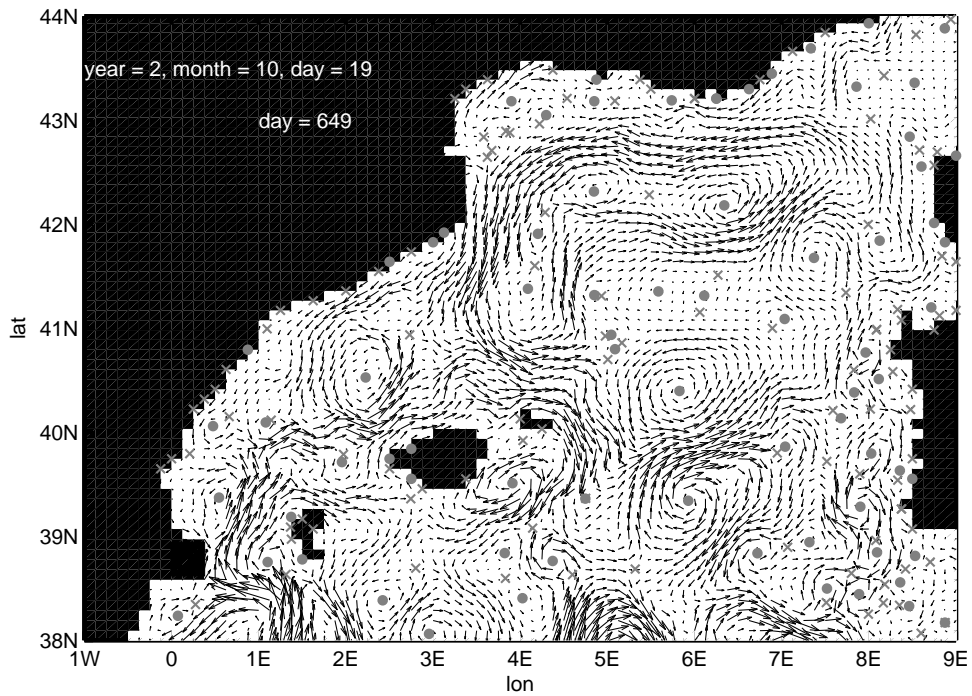


Figure 1: Velocity field at 15.93 m depth in the Northwestern Mediterranean at simulation day 649 (October). The Westernmost coast is the Spanish one, the islands are the Balearics, and the Easternmost coasts are portions of Corsica and Sardinia. Circles indicate elliptic ISPs and crosses indicate saddle-type ISPs.

tive velocities of 0.1-0.7 m/day, depending on location and season (d’Ovidio et al. 2004; Schneider et al. 2005), and thus residence times in the second layer are between two weeks and several months. As a rule of thumb we can consider that trajectories preserve two dimensionality during time intervals of about 20 days. Since most of our trajectory integrations will be restricted to time intervals below that duration, they can be considered two dimensional to a good approximation.

By inspection of the temperature and salinity model outputs we identify a four month interval starting on October of the second simulation year (i.e. Autumn and early Winter) as an example in which gradients are strong most of the time and thus the North Balearic Front well defined (see Fig. 2). We select this interval of time as our study case for which dynamic structures will be calculated.

## 4 Computation of Trajectories and Manifolds in Mediterranean Data Sets

The equations of motion that describe the horizontal evolution of particle trajectories in our velocity field are

$$\frac{d\phi}{dt} = \frac{u(\phi, \lambda, t)}{R \cos(\lambda)} \quad (1)$$

$$\frac{d\lambda}{dt} = \frac{v(\phi, \lambda, t)}{R} \quad (2)$$

where  $u$  and  $v$  represent the eastwards and northwards components of the surface velocity field coming from the simulations described in the previous section,  $R$  is the radius of the Earth (6400 km in our computations),  $\phi$  is longitude and  $\lambda$  latitude. Particle trajectories must be integrated in equations (1)-(2) and since information is provided just in a discrete space-time grid, a first issue to deal with is that of interpolation of discrete data sets. A recent paper by Mancho et al. (2006) compares different interpolation techniques in tracking particle trajectories. Bicubic spatial interpolation in space (Press et al. 1992) and third order Lagrange polynomials in time are shown to provide a computationally

efficient and accurate method. We use this technique in our computations. However we notice that bicubic spatial interpolation in space as discussed in Press et al. (1992) requires an equally spaced grid. Our data input is expressed in spherical coordinates, and the grid is not uniformly spaced in the latitude coordinate. In order to interpolate in an uniformly spaced grid, we transform our coordinate system  $(\lambda, \phi)$  to a new coordinate system with coordinates  $(\mu, \phi)$ . The latitude  $\lambda$  is related to the new coordinate  $\mu$

$$\mu = \ln|\sec\lambda + \tan\lambda| \quad (3)$$

Our velocity field is now on a uniform grid in the  $(\mu, \phi)$  coordinates. The equations of motion in the old variables are transformed to a new expression in the new variables,

$$\frac{d\phi}{dt} = \frac{u(\phi, \mu, t)}{R\cos(\lambda(\mu))} \quad (4)$$

$$\frac{d\mu}{dt} = \frac{v(\phi, \mu, t)}{R\cos(\lambda(\mu))} \quad (5)$$

where  $\lambda(\mu)$  is obtained by inverting Eq. (3), i.e.

$$\lambda = \frac{\pi}{2} - 2 \operatorname{atan}(e^{-\mu}) . \quad (6)$$

Once trajectories are integrated from these equations, for presentation purposes one can convert  $\mu$  values back to latitudes  $\lambda$  just by using (6).

Distinguished hyperbolic trajectories and their unstable and stable manifolds are the main dynamical systems objects that we use to describe and quantify transport. Our velocity data set lasts only for a finite time, it is highly aperiodic in time, and turbulent. Computation of hyperbolic trajectories for this kind of flow is discussed in Ju et al. (2003) and in Ide et al. (2002), where algorithms for their computation are developed. A novel technique to compute stable and unstable manifolds of hyperbolic trajectories in aperiodic flows is developed in Mancho et al. (2003). In Mancho et al. (2004) these hyperbolic trajectory and manifold computation algorithms are combined into a unified algorithm and successfully applied to a turbulent wind driven, quasigeostrophic double-gyre. We will now apply these same algorithms to compute hyperbolic trajectories and their stable

and unstable manifolds that we will use to describe and quantify transport associated with the North Balearic front.

## 5 Lagrangian structures and transport in the Balearic Sea

We focus on the region North of the Balearic Islands, the Balearic Sea. The main oceanic structures known to be present there are the Balearic current and the associated North Balearic Front (López-García et al. 1994; Millot 1999). This last feature is known to represent a transition zone between saltier and fresher waters in the Western Mediterranean. The salinity fields obtained from our computer simulation display significant salinity gradients (and also temperature gradients in Winter—in Summer the surface layer is heated in a rather homogeneous way) in the area (see Fig. 2). Our aim here is to interpret the presence of the gradients and the front in terms of a semipermanent “Lagrangian barrier” across which little transport occurs. This construction would also reveal the routes along which this transport happens. Topological changes in that picture, associated with the crossing by eddies and that may be interpreted as the breakdown of the front, are also observed during the simulation.

Gradients are rather well defined during Autumn of the second simulation year and early Winter of the third one. During this period we find a long interval (from day 649 to day 731) in which a Lagrangian structure constructed using stable and unstable manifolds of DHTs remains persistent and acts as a partial barrier to transport. Its location is well correlated with the salinity gradients, so that it can be interpreted as a Lagrangian identification of the North Balearic Front. The weak transport across the structure can be described in terms of lobe dynamics. The situation resembles the one in Coulliette and Wiggins (2001) in which quasigeostrophic dynamics has been used to model a double gyre situation and the central jet between the two gyres in that problem plays a similar role as that of the Balearic current in our problem. Lobe dynamics was there successfully applied to quantify transport across the jet, occurring by the so called turnstile mechanism. However in the more realistic data set analyzed here we need to

generalize some ideas used there. For example, in Coulliette and Wiggins (2001) DHTs stay on one dimensional boundaries for all time (as boundaries are invariant), however in our scenario the relevant current does not start nor end on clear one dimensional boundaries. This introduces some ambiguity in the identification of the relevant DHTs (and of the saddle-type ISPs used as starting positions in the iterative algorithm of (Mancho et al. 2004) that we use to determine the DHTs) from which to compute the manifolds that will define the Lagrangian barrier. Most of the time, however, pieces of manifolds computed from different DHTs in the same area rapidly converge towards each other, thus indicating that the location of the dominant hyperbolic curve is not a property of the particular choice of DHTs, but a property of the flow. Changes in the topology of the flow cause this convergence property to be lost. This happens at the end of the interval of time chosen in our study case and will be commented on below.

## 5.1 Cross frontal transport: the turnstile mechanism

The geometric objects used to characterize transport by lobe dynamics methods are constructed by the rules discussed in (Malhotra and Wiggins 1998; Coulliette and Wiggins 2001; Samelson and Wiggins 2006). Here we describe in some detail these procedures in a way that is particular to our flow situation. Figs. 2 - 4 illustrate the construction at days 649 and 657. Fig. 2 contains all the dynamic structures superimposed on a salinity field, whereas for clarity only the 'boundary' and the 'lobes' are displayed in Figs. 3, and 4, respectively.

1. Two DHTs should be identified, one in the western part of the front to be characterized and another in the eastern, that persists close to their initial positions during the whole time interval of interest (denoted by  $[t_0, t_N]$ ). Since our algorithm to locate DHTs uses saddle ISP positions as first guesses, figures displaying ISPs such as Fig. 1 are used to estimate these positions and the temporal persistence of the ISPs. The positions calculated for the selected DHTs are plotted in Figs. 2 - 6 as black dots and labelled as  $H_W$  (the western one) and  $H_E$  (the eastern one).

2. As the mean current flows eastwards we proceed as in Coulliette and Wiggins (2001) and compute the unstable manifold of the western DHT and the stable manifold of the one in the East. They are the red and blue lines in Fig. 2, respectively. For clarity in the presentation, of the two branches of each manifold (one at each side of the DHT from which they emanate) we display in Fig. 2 only the one pointing in the direction of the other DHT. Along both pieces of manifolds, in the region between the two DHTs, the dominant direction of motion is from west to east. As characteristic in unsteady flows, both manifolds intersect repeatedly. Some of the intersection points are marked with cyan dots. It is also typical that the unstable manifold (red) of a DHT ( $H_W$  in this case) emerges from it relatively straight, whereas it fluctuates widely when approaching the vicinity of the opposite DHT. In the same way, the stable manifold (blue) of  $H_E$  joins it smoothly, but displays characteristic oscillations when close to the western DHT. The stable and unstable manifolds displayed in Fig. 2 a) have been computed after backwards and forwards time integration of a small segment in the direction of the stable and unstable linear subspaces in the neighborhood of the DHT for time periods of 14 and 19 days, respectively. Integrations for longer time periods provide longer manifolds. However due to the restrictions of the two dimensional approximation, a time period beyond 20 days is not completely trustworthy. In practice this means that the pieces of the manifold that are far from the DHT may deviate from the true manifold as those pieces are the ones obtained with longer time integrations. For instance, the unstable manifold in Fig. 2 b) has been computed for a time integration of 27 days. This means that unstable structure in the far East is not completely reliable. However the piece of manifold governing the turnstile mechanism, which is closer to the DHT, is obtained with numerical integrations below the validity limit of 20 days and predictions obtained from them are correctly approached in the two dimensional approximation.
3. Between the beginning and the end of the chosen time interval, we choose a sequence of times at which to analyze the manifold positions and compute objects relevant for Lagrangian transport. The sequence of “observation times” is denoted

by  $t_0 < t_1 < t_2 < \dots < t_{N-1} < t_N$ . We note that the  $t_i$  do *not* need to be equally spaced. In order to illustrate the construction of boundaries and the turnstile mechanism for crossing the boundaries we need only two times, and for this purpose we will choose to show days 649 and 657.

4. At each of the selected times  $t_i$ , a “boundary” is constructed by choosing a finite piece of the unstable manifold of the western DHT,  $[H_W, b_{t_i}]$ , and a finite piece of the stable manifold of the eastern DHT,  $[b_{t_i}, H_E]$ , so that they intersect in precisely one point,  $b_{t_i}$ , which is called a *boundary intersection point*. The points  $\{b_{t_i}\}$ , in addition to satisfying an ordering constraint specified below, should be selected in such a way that a boundary relatively straight, i.e. free of the violent oscillations displayed by each of the manifolds when approaching the opposite DHT, is obtained. Since the boundary is pinned at the points  $H_W$  and  $H_E$  we obtain a sequence of boundaries that fluctuate in time but remain approximately in the same place. Figure 2 shows the selection of the boundary intersection points  $b_{649}$  and  $b_{657}$  at times 649 and 657, respectively. For clarity, Fig. 3 displays just the resulting boundaries.

Since the boundary is made of material lines, no fluid can cross it by horizontal advection processes, except at the observation times  $t_1, t_2, \dots, t_N$  at which the boundary is redefined. At these times, the only way fluid at one side of the boundary can be transferred to the other side is by the turnstile mechanism described and quantified below. If this transport amount is small (as it will be shown to be the case), the boundary can be characterized as a “barrier”, and gradients will be maintained across it. As seen in Fig. 2, the position of the boundary is well correlated with the position of the salinity front thus confirming that the dynamical systems techniques developed here are useful to identify the North Balearic front in terms of Lagrangian objects.

5. Construct turnstiles at  $t_i$ . At time  $t_i$  we consider the point, denoted by  $b_{t_{i+1}}^-$ , that will evolve into the boundary intersection point  $b_{t_{i+1}}$  (clearly, we cannot do this at  $t_N$ ). Since the stable and unstable manifolds are invariant, this point is also on both



the stable and unstable manifolds. In the same way,  $b_{t_{i-1}}^+$  is the location at time  $t_i$  of the boundary intersection point that was located at  $b_{t_{i-1}}$  at the previous time  $t_{i-1}$ . The additional constraint that needs to be imposed when choosing the sequence  $\{b_{t_i}\}$  is that  $b_{t_{i+1}}^-$  results “upstream” (i.e. closer to  $H_W$  along its unstable manifold, or further from  $H_E$  along its stable manifold) from  $b_{t_i}$ . This introduces a restriction on the choice of  $b_{t_{i+1}}$  once  $b_{t_i}$  is chosen. Since ordering of points along manifolds is preserved by time evolution, it turns out that  $b_{t_{i-1}}^+$  would be “downstream” from  $b_{t_i}$ . Figures 2, 3 and 4 display some of these intersection points, showing that our selection satisfies the ordering constraints. The segments of stable and unstable manifolds between  $b_{t_i}$  and  $b_{t_{i+1}}^-$  (and between  $b_{t_i}$  and  $b_{t_{i-1}}^+$ ) trap regions of fluid, and these regions of fluid defined in this way are referred to as *lobes*. Some of them can be seen in Fig. 2, and more clearly in Fig. 4.

6. Consider the evolution of the turnstile lobes from  $t_i$  to  $t_{i+1}$ . In this case  $b_{t_{i+1}}^-$  evolves to the boundary intersection point,  $b_{t_{i+1}}$ , and the boundary intersection point at  $t_i$  evolves to a point  $b_{t_i}^+$ , which is also on both the stable and unstable manifolds. Then the lobes between  $b_{t_{i+1}}$  and  $b_{t_i}^+$  represent the time evolution of the turnstile lobes from  $t_i$  to  $t_{i+1}$ . Note that, because of the way in which the boundary is redefined at each observation time, and because of the different shape of the manifolds when close or far from the DHT from which they emanate, each lobe is on opposite sides of the boundary at the two considered times. These turnstile lobes contain all the fluid that has crossed the boundary between  $t_i$  and  $t_{i+1}$ . This transport process is illustrated more clearly in Fig. 4 where the lobes experiencing the turnstile mechanism are plotted before and after crossing the boundary.

The geometric construction performed at every observation time  $t_i$  as explained above allows us to calculate the amount of transport occurring across the boundary during each time interval.

In computing the area  $A(\Gamma)$  of a lobe  $\Gamma$  we use the formula

$$A(\Gamma) = -R^2 \int_{\partial\Gamma} \sin \lambda d\phi \quad (7)$$

where the integration is around the closed curve which forms the boundary of the lobe. That this formula gives the area can be seen by considering the differential form  $\omega \equiv -R^2 \sin \lambda d\phi$ , calculating its differential (Spivak 1965):  $d\omega = R^2 \cos \lambda d\phi d\lambda$  which is identical to the area element on the sphere in spherical coordinates, and recalling Stokes theorem (Spivak 1965):

$$\int_{\partial\Gamma} \omega = \int_{\Gamma} d\omega. \quad (8)$$

For day 649, as shown in Fig. 4, the two turnstile lobes have areas of  $493.2 \text{ km}^2$  (the lobe below the boundary, to the east) and  $716.9 \text{ km}^2$  (the lobe to the west above the boundary). At day 657, the eastern lobe is above the new boundary, and the western lobe is below it. Assuming that the divergence of the surface flow can be neglected so that the areas are unchanged – in numerical experiments we have never observed more than a 3% change – we can calculate the flux across the barrier to be  $(716.9 - 493.2) \text{ km}^2 = 223.7 \text{ km}^2$ , in the southerly direction.

Modified Atlantic Waters occupy the surface layers of the area until an average depth of about 150m. Using as an approximation for the mean horizontal speed of this water mass the values at the second model layer considered here, multiplication of the 150m depth by the area of the lobes gives  $33.56 \times 10^9 \text{ m}^3$  in 8 days, or an average flux over this interval of 0,049 Sv ( $1 \text{ Sv} = 10^6 \text{ m}^3/\text{s}$ ). The average flux obtained from area calculations of further turnstile lobes until the middle of November remains below that value (the average is 0.025 Sv, always southwards). This should be compared to the 0.75-0.5 Sv which are transported by the Balearic current. We see that cross-boundary transport is small during this time interval and thus the Lagrangian boundary acts as a “barrier to transport” permitting only small amounts of mixing between Northern and Southern waters. It will maintain a salinity (and thus density) front that we identify with the observed North

Balearic front. There is some indeterminacy in the definition of the boundary that we identify as the front, arising from some freedom in the selection of the intersections  $\{b_{t_i}\}$ . But other choices can only displace the boundary by a distance of the order of the size of the lobes, which we see is small when not too close to the DHTs, and in fact also of the order of the width of the transition region in salinity distributions such as the one in Fig. 2, i.e. the width of the front.

## 5.2 Spatio-temporal structure of cross frontal transport

Since the only way in which our constructed Lagrangian boundaries can be crossed is via the turnstile mechanism, the earlier and later location of the turnstile lobes reveals the dominant routes along which the weak cross-front transport occurs. Figure 5 shows the time evolution of a pair of turnstile lobes, one initially above and the other initially below the boundary, as they evolve in time. The crossing of the boundary by the turnstile mechanism occurs between days 676 and 681, and the remaining panels in the figure show the position of these lobes at some earlier and later times. The sequence illustrate that lobes move essentially along the boundary except when close to  $H_E$ , where they are ejected as filaments transverse to the front (the one initially in the south ejected towards the north and reciprocally for the one started in the north) and when close to  $H_W$ , where they have also the shape of transverse filaments and they become entrained into the boundary region. Fig. 5 also illustrates how lobes transport water of different salinity (coded in colors) and how the above routes for lobe motion and shape correlate with the salinity distribution in the area. Note that the length of the manifolds and the whole process depicted in Fig. 5 lasts only 21 days, so that the plotted manifolds remain approximately horizontal, with only small corrections from the vertical flow.

## 5.3 An Eddy-front interaction: disruption of the Lagrangian boundary

Not all flow configurations allow the geometric construction identifying the Lagrangian boundary and the associated turnstile lobes to be performed. It may happen that no pair

of DHTs persist in a given area long enough to support the mechanism, or their manifolds can fail to intersect. It may also happen that manifolds started at relatively close DHTs do not converge to the same curve but remain significantly distinct, so that a unique well defined boundary can not be properly identified. In such cases, the turnstile transport mechanism is not the most relevant one. At the end of the simulation interval analyzed here we observe a change in the topology that signals the end of the predominance of the turnstile mechanism in a process that can be interpreted as the breakdown of the front by the interaction with an eddy. As a first symptom, calculations of turnstile lobe areas reveal an increase in cross-front transport starting at day 674 (middle of November). The average transport between days 674 and 700 is of 0.303 Sv (southwards), still smaller than the Balearic current transport but significantly larger than the average cross-frontal transport during the previous month (0.025 Sv, also southwards). At day 711, stable manifolds emerging from  $H_E$  and from another rather close DHT cease to converge into each other, signaling the end of a situation with an essentially unique well defined boundary. Later, at day 731 our algorithm is unable to find the location of  $H_E$  starting from ISPs in the area. This probably means that  $H_E$  has moved away from the area under study. The black dot in Fig. 6 is another DHT found in the region. But its stable manifold (i.e., the finite length of manifold that we are able to compute) does not intersect the unstable manifold from  $H_W$ , thus revealing that is in fact a DHT different from  $H_E$ , and that it can not support the turnstile mechanism. The time evolution of the unstable manifold from  $H_W$  suggests that the reason from the change in behavior is the breakdown of the Lagrangian barrier by the crossing of an eddy, identified by the rolling up of the manifold around an elliptic ISP (Fig. 6). Note that even in this situation the manifold position is well correlated with the salinity distribution, thus indicating that still Lagrangian structures are relevant. But the transport mechanism is clearly different from the turnstile described above, being more appropriately described as water transport inside an eddy.

## 6 Conclusions

In this work we have applied in a systematic way some tools developed in the context of dynamical systems theory and known generically as ‘lobe dynamics’. The computer generated surface velocity field studied here is more complex and less regular than other velocity fields previously considered in this context, but we have found that one of the main mechanisms of transport by lobe motion, the turnstile, is still at work. The methodology includes the construction of a ‘barrier’ across which to compute transport, and in our application to the Northwestern Mediterranean dynamics it has been identified with one of the main oceanographic structures present here, the North Balearic Front. Transport across it proceeds in the form of filaments that are entrained into the front close to a DHT ‘upstream’, and released also in the form of filaments close to another DHT located ‘downstream’. The ejection of these filaments at that location can explain recent observations of waters saltier than expected just east of the island of Menorca (Emelianov 2006). The identification of the DHTs and the calculation of their locations is by itself an important subject, since they organize the flow in the area and, because of this and of the sensitivity of the trajectories in their neighborhood, they are candidates for launch locations in efficiently designed drifter release experiments (Poje et al. 2002; Molcard et al. 2006).

Despite the success of the approach described here, much work remains to be done in order to develop dynamical systems techniques into a collection of systematic tools for analyzing general oceanographic data. A classification and understanding of the different topological regimes leading to qualitatively different modes of transport and the transitions among them, similar to the existing ones for steady and time-periodic flows, would be desirable for the cases of turbulent aperiodic flows. A characteristic of the dynamical systems approach is that it provides an unusually high detailed description of the spatio-temporal structure of Lagrangian transport. Therefore it may well turn out to be the optimal tool for analyzing data from ocean models with much higher spatio-temporal resolution (e.g., higher frequency atmospheric forcing and more resolved spatial scales)

which capture more physical processes. This would enable us to better define, for example, the process of the destruction of a barrier. In addition, consideration of the impact of non-Lagrangian processes such as diffusion, of vertical motions, and of strong localized perturbations beyond climatological forcing such as storms, would be needed to have a more complete vision of transport phenomena and mechanisms.

## Acknowledgements

A.M.M. acknowledges the MCyT (Spanish Government) for a Ramón y Cajal Research Fellowship and financial support from MEC (Spanish Government) reference MTM2004-00797 and the Royal Society-CSIC cooperation agreement reference B2003GB03. E.H.-G. acknowledges financial support from MEC and FEDER through Project CONOCE2 (FIS2004-00953). We also acknowledge M. Emelianov for communicating us results from a recent cruise before publication. D.S. and S. W. acknowledge financial support from ONR Grant No. N00014-01-1-0769.

## References

- Bartlett, J. H., 1982: Limits of stability for an area-preserving polynomial mapping. *Cel. Mech.*, **28**, 295–317.
- Beckers, J.-M., M. Rixen, P. Brasseur, J.-M. Brankart, A. Elmoussaoui, M. Crépon, Herbaut, F. Martel, F. V. den Berghe, L. Mortier, A. Lascaratos, P. Drakopoulos, G. Korres, K. Nit-tis, N. Pinardi, E. Masetti, S. Castellari, P. Carini, J. Tintoré, A. Álvarez, S. Monserrat, D. Parrilla, R. Vautard, and S. Speich, 2002: Model intercomparison in the Mediter-ranean: MEDMEX simulations of the seasonal cycle. *J. Mar. Sys.*, **33**, 215–251.
- Beigie, D., A. Leonard, and S. Wiggins, 1994: Invariant manifold templates for chaotic advection. *Chaos, Solitons, and Fractals*, **4(6)**, 749–868.

- Channon, S. R. and J. L. Lebowitz, 1980: Numerical experiments in stochasticity and homoclinic oscillations. *Ann. New York Acad. Sci.*, **357**, 108–118.
- Coulliette, C. and S. Wiggins, 2001: Intergyre transport in a wind-driven, quasi-geostrophic double gyre: An application of lobe dynamics. *Nonlinear Processes in Geophysics*, **8**, 69–94.
- Deese, H. E., L. J. Pratt, and K. R. Helfrich, 2002: A laboratory model of exchange and mixing between western boundary layers and subbasin recirculation gyres. *J. Phys. Oceanogr.*, **32(6)**, 1870–1889.
- Dietrich, D., 1997: Application of a modified “a” grid ocean model having reduced numerical dispersion to the Gulf of Mexico circulation. *Dyn. Atmos. Oceans*, **27**, 201–217.
- Dietrich, D., R. Haney, V. Fernández, S. Josey, and J. Tintoré, 2004: Air-sea fluxes based on observed annual cycle surface climatology and ocean model internal dynamics: a non-damping zero-phase-lag approach applied to the Mediterranean sea. *J. Mar. Sys.*, **52**, 145–165.
- d’Ovidio, F., V. Fernández, E. Hernández-García, and C. López, 2004: Mixing structures in the Mediterranean sea from finite-size Lyapunov exponents. *Geophys. Res. Lett.*, **31**, L12203 (1–4), doi:10.1029/2004GL020328.
- Duan, J. Q. and S. Wiggins, 1996: Fluid exchange across a meandering jet with quasi-periodic time variability. *J. Phys. Oceanogr.*, **26**, 1176–1188.
- Emelianov, M., 2006: Personal communication.
- Fernández, V., D. Dietrich, R. Haney, and J. Tintoré, 2005: Mesoscale, seasonal and inter-annual variability in the Mediterranean sea using a numerical ocean model. *Progress in Oceanography*, **66**, 321–340.

- Ide, K., D. Small, and S. Wiggins, 2002: Distinguished hyperbolic trajectories in time dependent fluid flows: analytical and computational approach for velocity fields defined as data sets. *Nonlinear Processes in Geophysics*, **9**, 237–263.
- Isern-Fontanet, J., García-Ladona, and J. Font, 2006: The vortices of the Mediterranean sea: an altimetric perspective. *J. Phys. Ocean.*, **36**, 87103.
- Jones, C. K. R. T. and S. Winkler, 2002: Invariant manifolds and Lagrangian dynamics in the ocean and atmosphere. *Handbook of dynamical systems*, North-Holland, Amsterdam, 55–92.
- Ju, N., D. Small, and S. Wiggins, 2003: Existence and computation of hyperbolic trajectories of aperiodically time-dependent vector fields and their approximations. *Int. J. Bif. Chaos*, **13**, 1449–1457.
- López-García, M., C. Millot, J. Font, and E. García-Ladona, 1994: Surface circulation variability in the Balearic Basin. *J. Geophys. Res.*, **99 (C2)**, 3285–3296.
- MacKay, R. S., J. D. Meiss, and I. C. Percival, 1984: Transport in Hamiltonian systems. *Physica D*, **13**, 55–81.
- Malhotra, N. and S. Wiggins, 1998: Geometric structures, lobe dynamics, and Lagrangian transport in flows with aperiodic time-dependence, with applications to Rossby wave flow. *J. Nonlinear Science*, **8**, 401–456.
- Mancho, A. M., D. Small, and S. Wiggins, 2004: Computation of hyperbolic and their stable and unstable manifolds for oceanographic flows represented as data sets. *Nonlinear Processes in Geophysics*, **11**, 17–33.
- 2006: A comparison of methods for interpolating chaotic flows from discrete velocity data. *Computers & Fluids*, **35**, 416–428.



- Mancho, A. M., D. Small, S. Wiggins, and K. Ide, 2003: Computation of stable and unstable manifolds of hyperbolic trajectories in two-dimensional, aperiodically time-dependent vector fields. *Physica D*, **182**, 188–222.
- Miller, P. D., L. J. Pratt, K. R. Helfrich, and C. K. R. T. Jones, 2002: Chaotic transport of mass and potential vorticity for an island recirculation. *J. Phys. Oceanogr.*, **32(1)**, 80–102.
- Millot, C., 1999: Circulation in the western Mediterranean sea. *J. Mar. Sys.*, **20**, 423–442.
- Molcard, A., A. Poje, and T. Özgökmen, 2006: Directed drifter launch strategies for Lagrangian data assimilation using hyperbolic trajectories. *Ocean Modell.*, **12**, 268–289.
- Ngan, K. and T. G. Shepherd, 1997: Chaotic mixing and transport in Rossby wave critical layers. *J. Fluid. Mech.*, **334**, 315–351.
- Olson, D., 1991: Rings in the ocean. *Annu. Rev. Earth Planet. Sci.*, **19**, 283–311.
- Pacanowski, R. C. and S. G. H. Philander, 1981: Parametrization of vertical mixing in numerical models of tropical oceans. *J. Phys. Oceanogr.*, **11(11)**, 1443–1451.
- Pinot, J. M., J. Tintoré, and D. Gomis, 1995: Multivariate analysis of the surface circulation in the Balearic sea. *Prog. Oceanogr.*, **36**, 343–376.
- Poje, A. C., M. Toner, A. D. Kirwan, and C. K. R. T. Jones, 2002: Drifter launch strategies based on Lagrangian templates. *J. Phys. Oceanogr.*, **32(6)**, 1855–1869.
- Press, W. H., S. A. Teukolsky, W. T. Vetterling, and B. P. Flannery, 1992: *Numerical Recipes in C*. Cambridge University Press.
- Puillat, I., I. Taupier-Letage, and C. Millot, 2002: Algerian eddies lifetime can be near 3 years. *J. Mar. Sys.*, **31**, 245–259.
- Rogerson, A. M., P. D. Miller, L. J. Pratt, and C. K. R. T. Jones, 1999: Lagrangian motion and fluid exchange in a barotropic meandering jet. *J. Phys. Oceanogr.*, **29**, 2635–2655.

- Rom-Kedar, V., A. Leonard, and S. Wiggins, 1990: An analytical study of transport, mixing, and chaos in an unsteady vortical flow. *J. Fluid Mech.*, **214**, 347–394.
- Rom-Kedar, V. and S. Wiggins, 1990: Transport in two-dimensional maps. *Arch. Rat. Mech. Anal.*, **109**, 239–298.
- Ruiz, S., J. Font, M. Emelianov, J. Isern-Fontanet, C. Millot, J. Salas, and I. Taupier-Letage, 2002: Deep structure of an open sea eddy in the Algerian Basin. *J. Mar. Sys.*, **33–34**, 179–195.
- Samelson, R. and S. Wiggins, 2006: *Lagrangian Transport in Geophysical Jets and Waves*. Springer-Verlag, New York.
- Samelson, R. M., 1992: Fluid exchange across a meandering jet. *J. Phys. Oceanogr.*, **22**, 431–440.
- Sanderson, B. and G. Brassington, 1998: Accuracy in the context of a control-volume model. *Atmosphere-Ocean*, **36**, 355–384.
- Schneider, J., V. Fernández, and Hernández-García, 2005: Leaking method approach to surface transport in the Mediterranean sea from a numerical ocean model. *J. Mar. Sys.*, **57**, 111–126.
- Spivak, M., 1965: *Calculus on Manifolds*. Perseus Books, New York.
- Wiggins, S., 1992: *Chaotic Transport in Dynamical Systems*. Springer-Verlag, New York.
- 2005: The dynamical systems approach to Lagrangian transport in oceanic flows. *Annu. Rev. Fluid Mech.*, **37**, 295–328.
- Yuan, G.-C., L. J. Pratt, and C. K. R. T. Jones, 2001: Barrier destruction and Lagrangian predictability at depth in a meandering jet. *Dyn. Atmos. Oceans*, **35**, 41–61.
- 2004: Cross-jet Lagrangian transport and mixing in a  $2\frac{1}{2}$  layer model. *J. Phys. Oceanogr.*, **34**, 1991–2005.

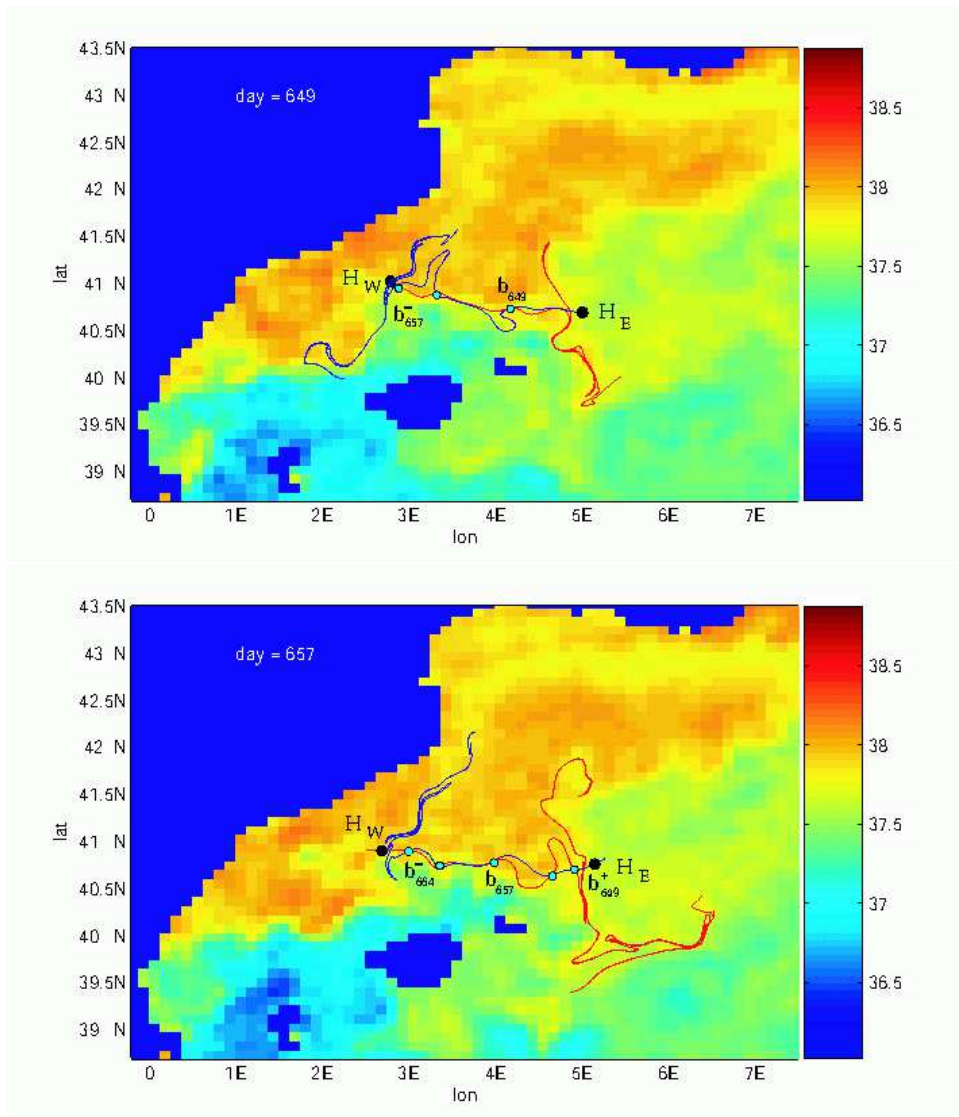


Figure 2: Salinity front and manifolds at days 649 and 657. Salinity (in psu) is color coded as indicated by the color bar. The black circles denote the DHT in the West ( $H_W$ ) and the DHT in the East ( $H_E$ ). These are the DHTs whose unstable (red) and stable (blue) manifolds, respectively, are used to construct the Lagrangian boundary of the front. The blue dots are boundary intersection points, as described in the text.

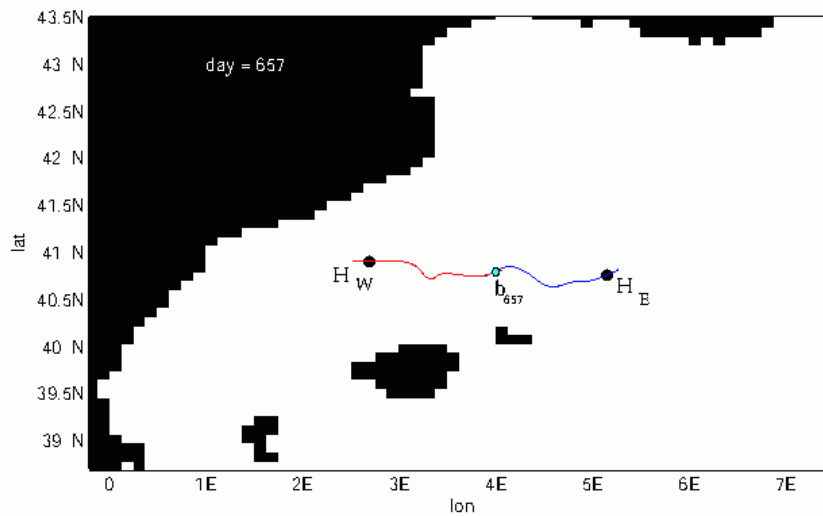
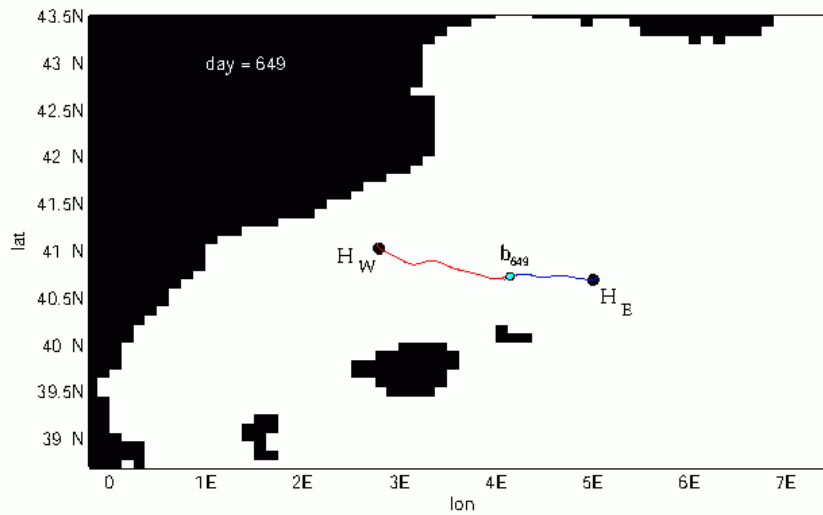


Figure 3: Boundaries at days 649 and 657 constructed from a (finite length) segment of the unstable manifold of  $H_W$  and a (finite length) segment of the stable manifold of  $H_E$ . The boundary intersection points are denoted by  $b_{649}$  and  $b_{657}$ , respectively.

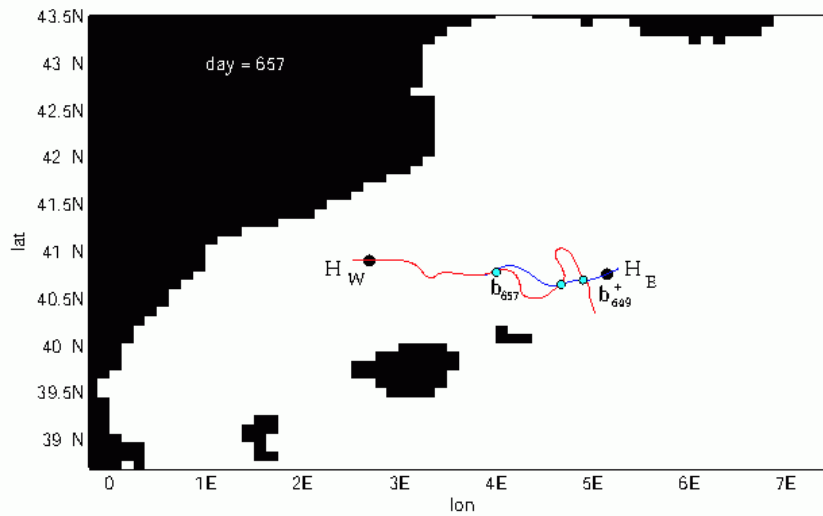
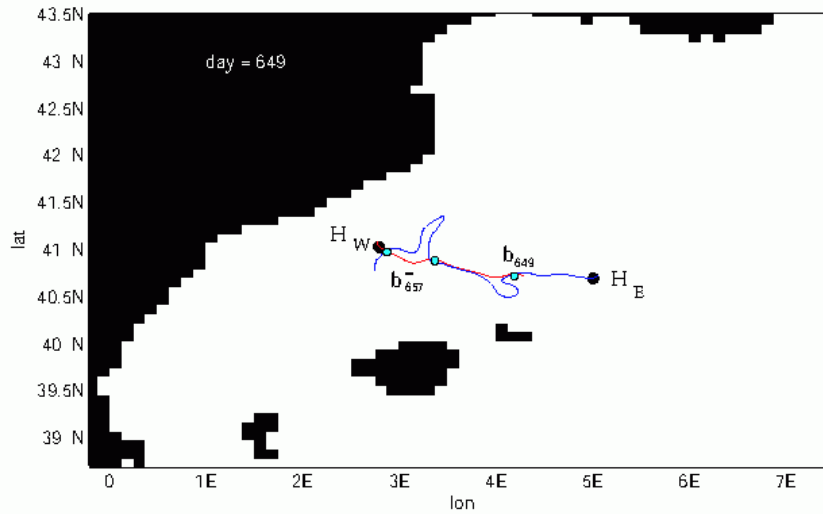
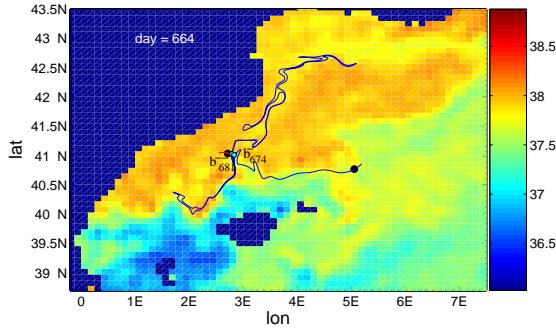
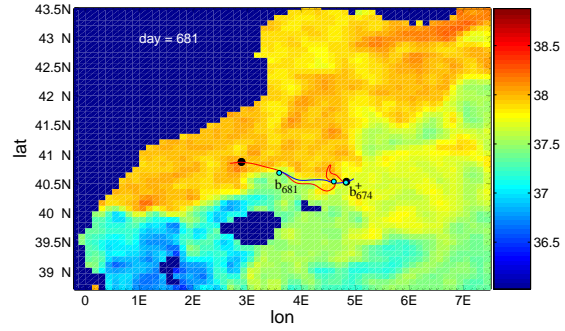


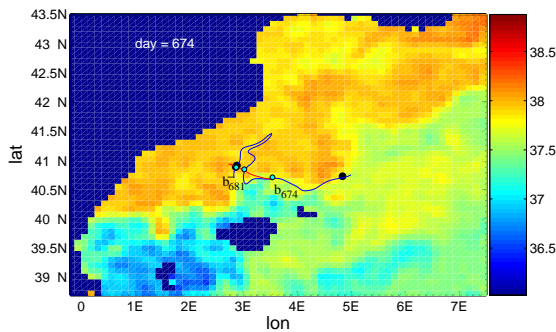
Figure 4: Turnstile lobes from day 649. There is precisely one intersection point between  $b_{649}$  and  $b_{657}^-$ , which implies that there are two lobes in the turnstile. The bottom figure shows the evolved position of these lobes at day 657. Comparing the two figures, one can see that the turnstile lobe to the North of the boundary at day 649 has moved to the South of the boundary at day 657, and the turnstile lobe to the South of the boundary at day 649 has moved to the North of the boundary at day 657 (the location of the boundary itself can be seen in Fig. 3).



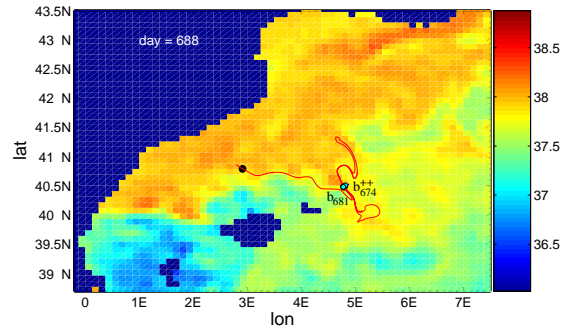
(a) Evolution of the turnstile lobes at day 674 backwards in time to day 667, or, in other words, the location on day 667 of the lobes that are turnstile lobes at day 674. The notation  $b_{681}^{-}$  denotes the evolution of the boundary intersection point at day 681 *backwards* two observation times (to day 674 and to the current time, day 667).



(c) The turnstile lobes evolved to day 681.

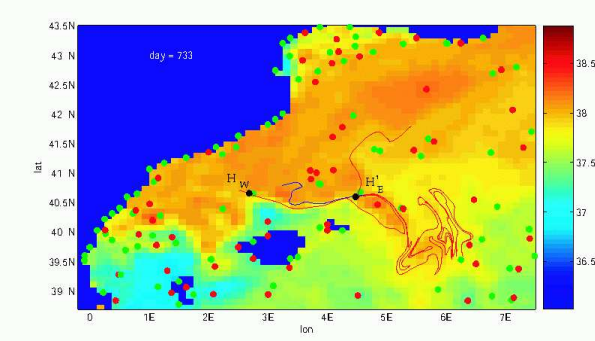


(b) Turnstile lobes at day 674.

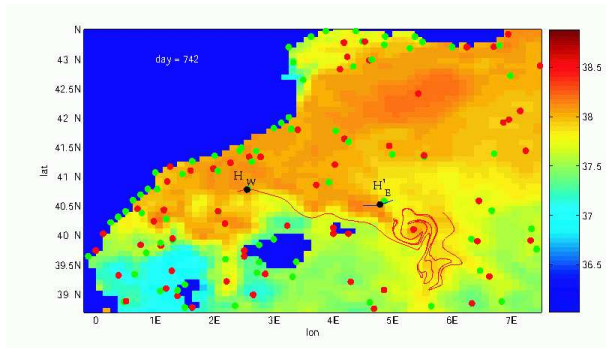


(d) The turnstile lobes evolved to day 688. The notation  $b_{674}^{++}$  denotes the evolution of the boundary intersection point at day 674 *forwards* two observation times (to day 681 and to the current time, day 688).

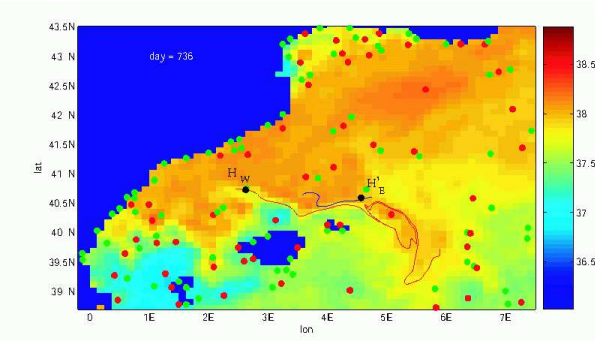
Figure 5: The spatio-temporal structure of cross frontal transport described by lobe dynamics. Salinity (in psu) is color coded as indicated by the color bar.



(a) Day 733. The unstable manifold of  $H_W$  does not appear to intersect the stable manifold of  $H'_E$ . The unstable manifold is strongly influenced by the circulation associated with the elliptic ISP immediately to the lower right of  $H'_E$ .



(c) Day 742. The earlier Lagrangian barrier now appears completely destroyed as a result of the influence of the eddy.



(b) Day 736. As the elliptic ISP moves further away from  $H'_E$  its influence carries the unstable manifold with it.

Figure 6: The mechanism of the disruption of the Lagrangian barrier by an eddy. Salinity (in psu) is coded in colors as indicated by the color bar. Red dots are ISPs of elliptic character. Green dots are saddle ISPs. Also shown as black dots are the DHTs  $H_W$  and  $H'_E$ .